Soft Matter

The Influence of Spacer Composition on Thermomechanical Properties, Crystallinity, and Morphology in Ionene Segmented Copolymers

Journal:	*Soft Matter*
Manuscript ID	SM-ART-04-2021-000501.R1
Article Type:	Paper
Date Submitted by the Author:	30-Apr-2021
Complete List of Authors:	Liesen, Nicholas; The Ohio State University Wang, Meng; Arizona State University Taghavimehr, Mehrnoosh ; Iowa State University Lee, Jae Sang; Arizona State University, Chemical Engineering Montazami, Reza; Iowa State University, Department of Mechanical Engineering Hall, Lisa; The Ohio State University, Green, Matthew; Arizona State University, Chemical Engineering

The Influence of Spacer Composition on Thermomechanical Properties, Crystallinity, and Morphology in Ionene Segmented Copolymers

Nicholas Liesen,[a§] Meng Wang,[b§] Mehrnoosh Taghavimehr,[c§] Jae Sang Lee,[d] Reza Montazami,*[c] Lisa M. Hall,*[a] and Matthew D. Green*[d]

[a]Department of Chemical and Biomolecular Engineering, The Ohio State University, Columbus, OH 43221, USA
[b]School of Molecular Science, Arizona State University, Tempe, AZ 85281, USA
[c]Department of Mechanical Engineering, Iowa State University, Ames, IA 50011, USA
[d]Department of Chemical Engineering, School for Engineering of Matter, Transport and Energy, Arizona State University, Tempe, AZ 85287, USA
[§]Co-first authors
*Co-corresponding authors: E-mail address: reza@iastate.edu, hall.1004@osu.edu, and mdgreen8@asu.edu

Keywords: Ionenes, segmented copolymers, molecular dynamics, thermomechanical properties

For Table of Contents Use:

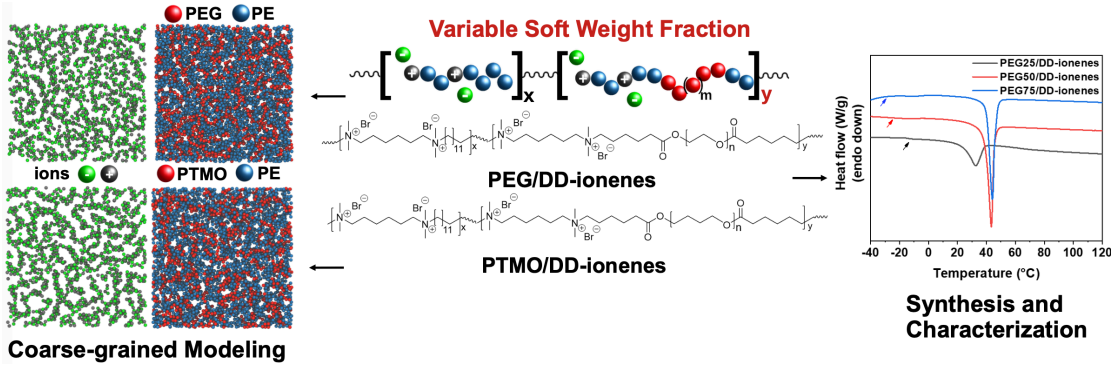

Abstract

A series of segmented ammonium ionenes with varying weight fractions of 2,000 g/mol poly(ethylene glycol) (PEG) or poly(tetramethylene oxide) (PTMO) soft segments were synthesized, and a simplified coarse-grained model of these materials was

implemented using molecular dynamics simulations. In addition to varying soft segment type (PTMO vs. PEG), charge density and soft segment content were varied to create a comprehensive series of segmented ammonium ionenes; thermogravimetric analysis reveals that all segmented ionenes in the series are thermally stable up to 240 °C. Differential scanning calorimetry (DSC) and dynamic mechanical analysis (DMA) show the formation of phase separated microdomains at low soft segment content. In particular, DSC shows that the hard and soft domains have distinct glass transition temperatures. Similarly, simulations show that reduced soft segment content induces stronger microphase separation, reduces soft segment mobility, and increases ionic aggregate connectivity and size. These increased ionic associations result in elastomeric behavior, as evidenced by the higher rubbery plateau moduli observed at lower soft segment contents through DMA. Moreover, simulations show that ionic aggregation increases when switching from PEG to the less polar PTMO repeat units, which is consistent with DMA results showing higher plateau moduli for PTMO-based ionenes relative to PEG ionenes. DSC and X-ray diffraction determined that the degree of crystallinity increased with soft segment content regardless of segment type. Overall, these results suggest a semi-crystalline microphase-separated morphology strongly influenced by charge density, the degree of ionic aggregation, and the resulting level of confinement and mobility of the soft segments.

Introduction

Ionenes are a class of charge-containing polymers wherein the ion is contained within the polymer backbone, rather than attached to pendant groups along the polymer

backbone. This configurational alteration yields unique morphological and electrostatic characteristics to the polymer. For example, ionenes can exhibit precise ion-spacing along the polymer backbone in spite of broad molecular weight distributions. This attribute gives rise to microstructures akin to semi-crystalline polyurethanes (described in more detail later). Additionally, the charge aggregates and ionic microdomains can create elastomeric networks, depending on the length and flexibility of the non-ionic spacers. In other words, ionenes present a unique material set to tune the properties and characteristics of the polymer.

Ionenes are synthesized through step-growth type polymerizations, which provides straightforward pathways to synthesize segmented or multi-block copolymers. To provide context, polyurethanes are the class of polymer most commonly associated with segmented or multi-block copolymers, which, as a class, routinely display robust and tunable elastomeric thermomechanical properties and interesting microstructural features. The chemical dissimilarities between the urethane linkages (the hard segments) and the soft segments (commonly polyethers) cause phase separation.[1] The thermal and mechanical properties are dramatically influenced by the extent of phase separation and the microphase morphology. Substituting the urethane-based hard segments with ionic hard segments captures many of the same material characteristics including microphase separation and the elasticity of a thermoplastic elastomer.

Segmented ionenes have been synthesized and studied recently by several groups. Leir and Stark reported the synthesis of segmented ionenes using α,ω-bis(dimethylamino) poly(tetramethylene oxide) and various dihalides; they observed

that the structure of the dihalide was important both for the polymerization kinetics and the thermomechanical properties of the polymers.[2] Similarly, Feng et al. investigated the ionenes made by Leir and Stark above, but also explored the effect of the PTMO segment length on the properties of the ionenes.[3,4] Small-angle X-ray scattering (SAXS) and transmission electron microscopy (TEM) were used to determine that the ionic domains microphase separated from the PTMO segments into thin, needle-like microdomains. They also determined that decreasing the PTMO soft segment molecular weight improved the mechanical properties by increasing the density of ionic associations and creating stronger physical crosslinks. Counterion size and shape can also alter the ionic aggregation behavior and resulting mechanical and thermal properties as well as the degree of microphase separation.[5] Loveday et al. reported that PTMO-based ionenes with Br^- counterions showed better phase separation when compared to PF_6^- counterions; the counterion size and electron density played a role in dictating the morphology.[6] Ikeda et al. reported the effect of counterion type on the morphology of PTMO-based ionenes by showing that the subtle change from the chloride to the bromide counterion reduced the size of the ionic domains.[7]

In segmented ionenes, phase separation contributes to the mechanical performance and it has been shown that the stress-strain behavior is dominated by the soft segment structure and properties. Robbins et al. noted that ionenes with bromide counterions displayed better mechanical performance when compared to ionenes with chloride counterions.[8] Long and coworkers studied a series of linear and highly branched PTMO-based ionenes and determined that branched soft segments prevented ionic

aggregation regardless of the PTMO segment molecular weight and that the polymer architecture did not influence the soft segment T_g.[9] For ionenes with a linear PTMO soft segment, robust thermomechanical properties with a rubbery plateau that persisted until ~175 ˚C were observed. Interestingly, non-segmented ammonium ionenes have been shown to have a relatively low cytotoxicity.[10] This suggests that using PEG-based segmented ionenes for biomedical applications is possible since other PEG-containing polymers are known to have good biocompatibility and low biotoxicity.[11] Sukhyy and coworkers recently reported the synthesis, thermal properties, and ionic conductivity of novel PEG-based ionenes.[12] By increasing the PEG molecular weight they were able to decrease the charge density as well as the T_g. Moreover, segmented PEG ionenes can be used in electronic devices to tune the ionic conductivity through changes in the molecular weight of PEG soft segments, which influences the ion mobility and volume fraction of the conducting phase.[12] For example, Thankamony et al. prepared a polymer electrolyte using segmented ionenes with imidazolium-based hard segments and PEG soft segments for Li^+ battery applications.[13] Collectively, these accounts highlight the need for a deeper understanding into the effects of the soft segment composition on the thermomechanical properties and morphology of segmented ionenes.

While there has been relatively less simulation work specifically focused on segmented ionenes,[14] many prior theoretical and simulation studies have made progress in understanding how polymer architecture, local phase segregation, and ionic aggregation impact material properties in a variety of dry ionomer systems, including ionenes in some cases. In particular, a number of studies used coarse-grained molecular

dynamics (MD) simulations to consider simple ionomers with uncharged backbones of a single chemical type and ions either within the backbone (ionenes) or pendant to the backbone.[15–17] Together with experimental work on related ionomers with precisely controlled spacing of ionic groups and with atomistic MD simulations,[18] the prior work shows that polymer architecture, including the fractional ion content and spacing between ionic groups along the chain, is crucial in determining the ionic aggregate morphology and the resultant material properties.[19] It is clear that the dielectric constant of the polymer medium is also a key factor. Essentially all ions were found to participate in ionic aggregates (which can be either small and compact or stringlike depending on polymer architecture) at a dielectric constant ϵ_r of 2-4 similar to that of a polyethylene (PE) backbone; however, at higher ϵ_r of 8-10 more representative of PEG, more free ions exist, and aggregates are smaller regardless of polymer architecture.[16,17] It is important to note that much of the prior coarse-grained MD studies on dry ionomers mentioned above focused on the relatively low ϵ_r systems with more significant and longer-ranged ionic aggregation than the systems of interest in the current paper, and the current systems include the additional complication of chemically different polymer backbone segments that can locally microphase segregate. In terms of segmented ionene simulations, our work here builds directly on our prior coarse-grained MD study on a series of segmented ionenes with varying amounts of poly(propylene glycol) (PPG) soft segments.[14] In this simple model, ϵ_r was considered constant throughout the simulation box, as in other prior coarse-grained work. Due to the importance of ϵ_r in determining ionic aggregation, it is important to adjust this background value based on

the types of polymer segments used. Thus, ϵ_r was set at a value based on a weighted average of the dielectric constants of the components of the system. We follow the same approach here, with further details discussed in the methods section. Changing weight fraction of PPG was shown to lead to significant changes in local microphase segregation and ionic aggregation, and the related changes in polymer relaxation times were also analyzed.[14]

In this work, we employ both experiments and simulations to study a series of segmented ionenes with two types of soft segments and several soft segment weight fractions. Specifically, a 2,000 g/mol dibromo-PEG or dibromo-PTMO soft segment was copolymerized with 1,12-dibromododecane and N,N,N',N'-bis(dimethylamino)hexane to create segmented ammonium ionenes. The thermal, mechanical, and morphological attributes of the ionenes were investigated. Experimental characterization shows that soft segment composition has a strong effect on the degree of crystallinity, which influences modulus and ultimate mechanical behavior. Coarse-grained MD simulations allow us to further examine the connection between soft segment weight fraction and microphase and ionic aggregate structure in these ammonium ionenes.

Results and Discussion

Synthesis and characterization of PEG-based and PTMO-based ammonium ionenes with varying hard segment content

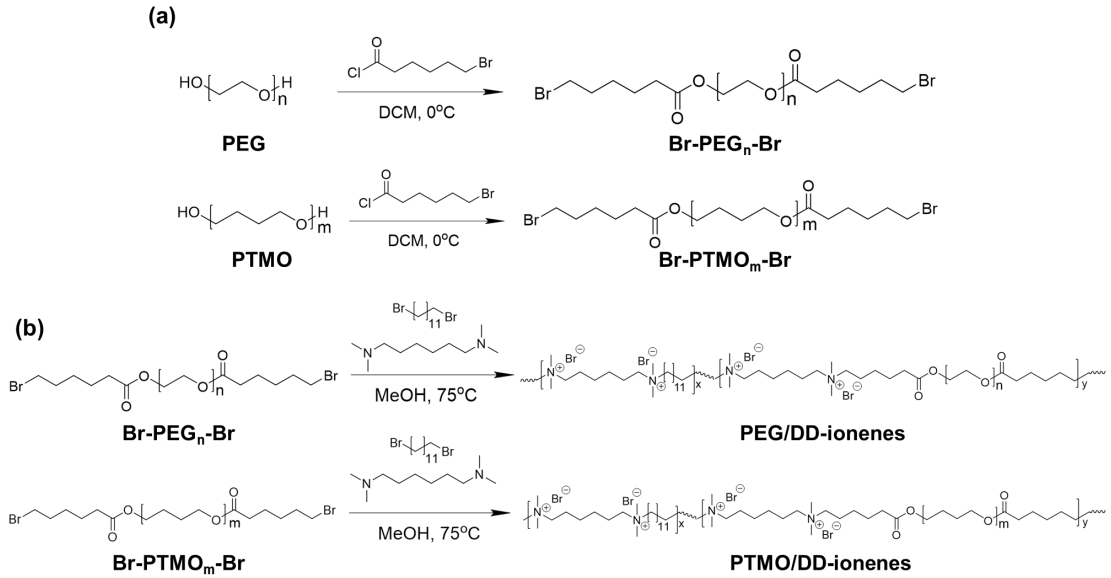

Scheme 1. The synthesis of (a) Br-PEG_n-Br and Br-$PTMO_m$-Br, and (b) PEG/DD-ionenes and PTMO/DD-ionenes

Two series of segmented ionenes possessing a varying charge content (and therefore hard segment weight fraction) for two different soft segment compositions were synthesized via step-growth polymerization. First, PEG-based ionenes were synthesized by polymerizing N,N,N',N'-tetramethyl-1,6-hexanediamine with varying ratios of bromine end-capped PEG (Br-PEG_n-Br) and Br-$C_{12}H_{24}$-Br (dodecane dibromide, DD). Second, PTMO-based ionenes were synthesized by polymerizing N,N,N',N'-tetramethyl-1,6-hexanediamine with varying ratios of bromine end-capped PTMO (Br-$PTMO_m$-Br) and DD. In all cases, the Br:N molar ratio was kept at 1:1 to target a high polymer molecular weight; the reaction proceeded for 24 h (**Scheme 1**). This design creates segmented or multi-block copolymers with soft PEG or PTMO segments separated by ionic hard segments comprised of the N,N,N',N'-tetramethyl-1,6-hexanediamine and DD moieties. We have defined the following nomenclature for the two series of polymers: PEGXX/DD-ionene and PTMOYY/DD-ionene. The XX or

YY indicates the overall weight fraction of the PEG or PTMO in the multiblock copolymer, respectively.

The chemical structure of the ionenes was confirmed using ^{1}H-NMR spectroscopy (**Figure 1**). The peak just below 3.4 ppm in both sets of spectra represents the methylene protons attached to the quaternary ammonium group, which signifies a successful polymerization. The peaks in the range of 1.0–2.5 ppm are attributed to the methylene protons from the N,N,N',N'-tetramethyl-1,6-hexanediamine and the DD moieties, which increase in intensity relative to the peak at 3.4 ppm as the PEG or PTMO weight fraction decreases. Finally, the peak at 3.6 ppm in **Figure 1a** and the peaks at 1.6 and 3.4 ppm in **Figure 1b** are attributed to the methylene protons from the PEG and PTMO soft segments.

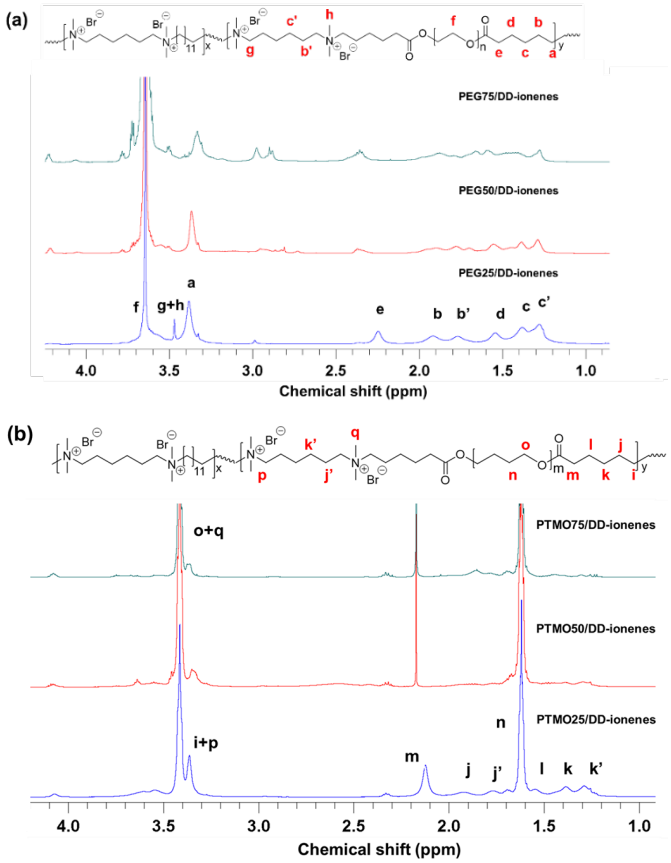

Figure 1: ^{1}H-NMR spectra for (a) PEG/DD-ionenes with varying PEG weight fractions and (b) PTMO/DD-ionenes with varying PTMO weight fractions.

Effect of hard segment content on the thermal properties of segmented PEG-based and PTMO-based ionenes.

The thermal stability of ionenes is dependent on the basicity of the counterion and the hard segment content. The PEGXX/DD-ionene series exhibited a weight loss at approximately 240 ˚C (**Figure 2a**) that was inversely proportional to the PEG weight fraction in the polymer. The mechanism for thermal degradation of ionenes is commonly accepted to follow the Hoffman elimination mechanism.[20] More specifically, the halide counterion is sufficiently basic enough to abstract a proton from the methylene group in the beta position relative to the ammonium cation causing chain scission and the creation of unsaturated bonds. In the case of ionenes, this causes depolymerization and volatilization of small molecule amines and hydrocarbons but

leaves behind the soft segment in segmented multiblock copolymers. Thus, the segmented ionenes degraded in two distinct steps: the first weight loss corresponds to the weight percentage of the hard segment, and the second weight loss corresponds to the weight percentage of the soft segment. The same trend was observed for the PTMOYY/DD-ionene series (**Figure 2b**). Interestingly, the soft segment degradation temperature for the PTMOYY/DD-ionene series occurred at a slightly higher temperature (~425 ˚C) when compared to the neat PTMO (~350 ˚C).

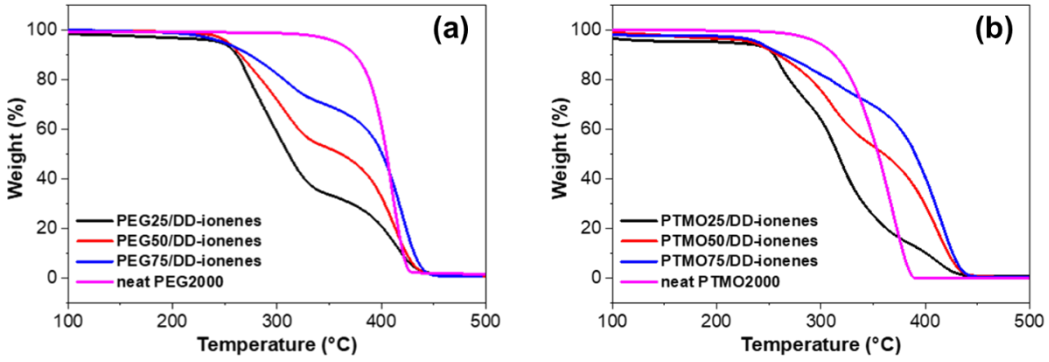

Figure 2: TGA overlays of (a) PEGXX/DD-ionenes compared to neat PEG, and (b) PTMOYY/DD-ionenes compared to neat PTMO.

DSC was used to study the thermal transitions within the PEG/DD-ionenes and the PTMO/DD-ionenes. We expected to observe a soft segment glass transition from the PEG or PTMO phase, a melting transition from the PEG or PTMO crystallites, and a hard segment glass transition. First, the trends in the number and values of the T_gs are analyzed. All of the PEG/DD-ionenes exhibited a T_g in the range of -20 – -13 ˚C, which corresponded to the T_g of the PEG soft segment. These values are higher than the typical T_g of PEG (about -40 ˚C), indicating restrictions on chain mobility caused by the form of the multiblock copolymer. The PEG25/DD-ionene exhibited a second T_g at 62 ˚C as

well. This behavior could be due to microphase separation to form a PEG-rich soft microphase and an ion-rich hard microphase. The appearance of this second T_g is qualitatively consistent with the MD simulation results below, where radial distribution functions (**Figure 6** and **Figure 8**) and the partial structure factor for PE and PEG (**Figure 7** and **Figure 9**) show increasing microphase separation as hard segment content increases. Decreasing the soft segment weight fraction increases the charge density, which has been shown to increase a polymer's T_g.[21] This increase in charge density acts to reduce the mobility of the PEG domains. We also observe the trend that decreasing the weight fraction of the soft segment increases the T_g of PEG domain from -30 °C for the PEG75/DD-ionene to -13 °C for the PEG25/DD-ionene system (**Figure 3a, e**). Simulation results are generally consistent with these observations, with the self-intermediate structure factor (**Figure 13**) indicating that repeating unit relaxation times for PEG decrease as the soft segment weight fraction increases. This suggests reduced mobility of the PEG repeat units in the lower weight fraction systems, likely due to an increase in ionic aggregation reduced mobility of segments near the aggregates. However, it should be noted that these simulations were not cooled below the T_g (simulations are run at a reduced temperature of T^*=1.2, which corresponds to 360 K). These effects, increasing charge density and reduced mobility, increase the T_g of the soft segment. The PTMOYY/DD-ionene series displayed different behavior (**Figure 3b, e)**. The PTMO soft segment should exhibit a T_g around -80 °C, which is below our experimental capabilities for DSC. However, the PTMO/DD-ionene series exhibited a hard segment glass transition for two samples: the PTMO25/DD-ionene (at 120 ˚C) and

the PTMO50/DD-ionene (at 60 ˚C). As was the case with PEGXX/DD-ionenes, MD simulations of PTMOYY/DD-ionenes show decreasing microphase separation with increasing PTMO content, as will be further discussed below (see the radial distribution functions and partial structure factors in Error! Reference source not found. **8 and** Error! Reference source not found. **9**). This is qualitatively consistent with the disappearance of the second glass transition temperature in the highest soft segment content system.

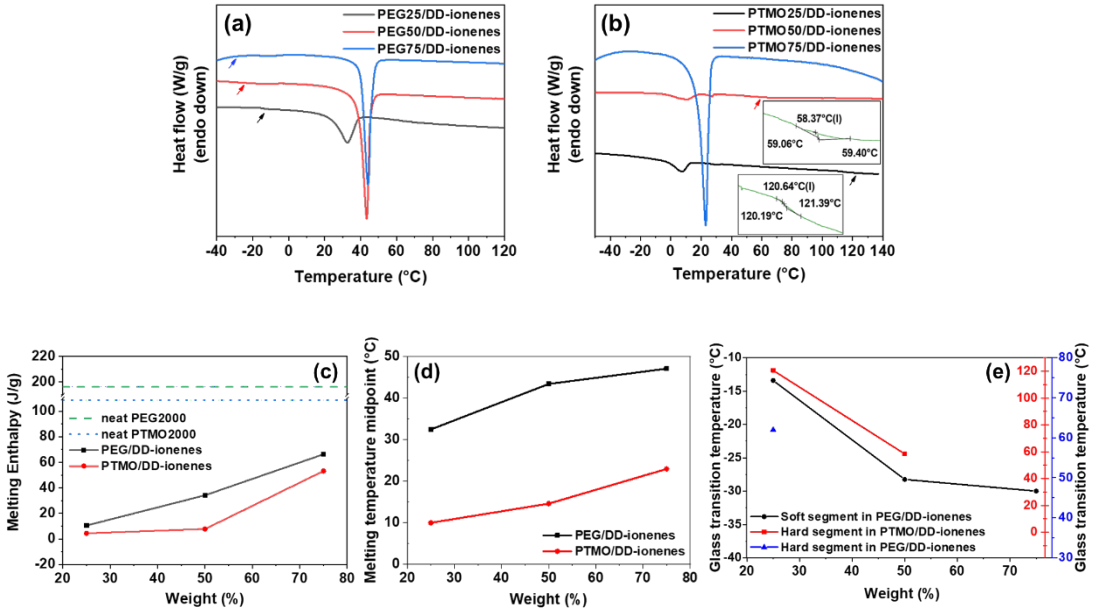

Figure 3: DSC results for (a) PEG/DD-ionenes and (b) PTMO/DD-ionenes. DSC was used to determine the (c) melting enthalpy of PEG/DD-ionenes and PTMO/DD-ionenes relative to the neat PEG or PTMO soft segment, (d) the midpoint T_m of PEG/DD-ionenes and PTMO/DD-ionenes, as well as (e) the T_g of the soft segment in PEG/DD-ionenes and the hard segment in PTMO/DD-ionenes and PEG/DD-ionenes.

Next, the trends in the melting transitions for the PEG/DD-ionenes and PTMO/DD-ionenes were analyzed (**Figure 3a, b, c, d**). A direct correlation between the melting enthalpy and the weight fraction of the soft segment was observed for the PEG/DD-ionene and PTMO/DD-ionene series. This is expected since there is a higher concentration of the moieties that can crystallize. However, for the PEG/DD-ionenes

the melting enthalpy increases at a greater rate than the soft segment weight fraction (e.g., the melting enthalpy is ~3.5× higher at 50 wt% soft segment relative to 25 wt% soft segment and ~1.8× higher at 75 wt% soft segment relative to 50 wt% soft segment). This suggests that the higher soft segment weight fractions provide more configurational freedom, which increases the degree of crystallization. This phenomenon also led to an increase in the melting temperature of soft segment crystallite, which is suggestive of purer crystallites. The trend for the PTMO/DD-ionene series is different; increasing the soft segment weight fraction from PTMO25/DD-ionene to PTMO50/DD-ionene caused very little increase in the melting enthalpy. However, the increase from PTMO50/DD-ionene to PTMO75/DD-ionene caused an ~10× increase in the melting enthalpy. This behavior suggests that some threshold exists with significantly different interfacial and microstructural characteristics at lower (<50 wt%) vs. higher (>50 wt%) soft segment weight fractions. Moreover, the PEGXX/DD-ionene's melting temperatures (>32 ˚C) are consistently higher than those of the PTMOYY/DD-ionenes (which are consistently at or below room temperature). Thus, the small melting enthalpies for the lower weight fractions of the PTMO soft segment are sensible. Note that the MD simulations were performed in the melt state and used a simple coarse-grained model that does not crystallize, thus, we do not directly compare simulation results to melting temperatures or enthalpies.

The crystalline properties of the segmented ionene copolymers were further investigated by X-ray Diffraction (XRD). As noted above, the melting temperature of the PTMO-based ionenes was at or below room temperature, which likely influenced

the XRD results because the PTMO crystallites could melt during the test. The XRD patterns for the PEGXX/DD-ionenes and PTMOYY/DD-ionenes are shown in **Figure 4**. The two prominent peaks for PEG (at 2θ = 19.2˚ and 23.4˚, at q = 1.35 and 1.64) were present in the diffraction patterns when the PEG soft segment weight fraction was greater than 50 wt%. The PTMO XRD diffraction patterns showed peaks at q = 1.41 and 1.72 (2θ = 19.5˚ and 24.0˚), which were observed in the diffraction patterns for the PTMO/DD-ionenes when the soft segment weight fraction was >75 wt%. These data corroborate the findings from DSC, that the degree of crystallinity, and hence the diffraction intensity, increases with the soft segment weight fraction.

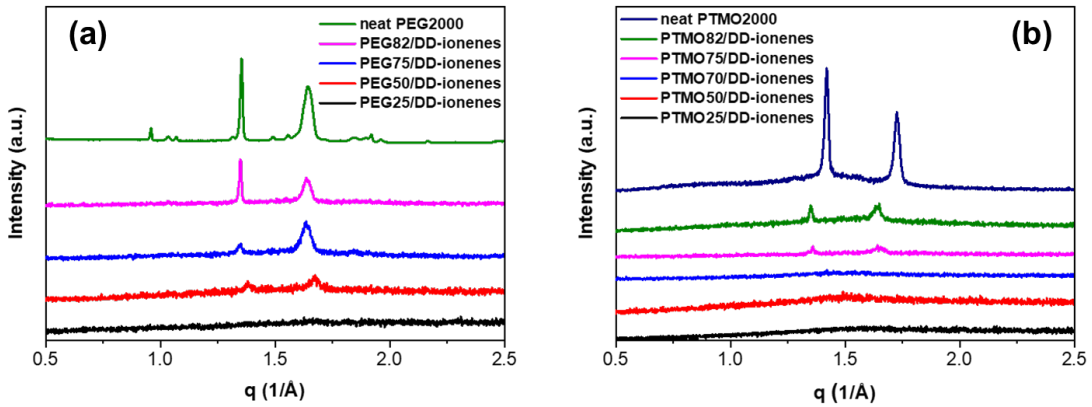

Figure 4: Overlayed XRD result of (a) PEG/DD-ionenes with different hard segment weight fractions and (b) overlayed XRD result for PTMO/DD-ionenes with different hard segment weight fractions.

Effect of hard segment content on the mechanical properties of segmented PEG-based and PTMO-based ionenes.

The mechanical properties of ionenes are strongly affected by the weight fractions of the soft and hard segments. Higher soft segment contents result in a more crystalline structure, to a point that the ionene cannot be fabricated into a robust thin-film that is suitable for dynamic mechanical analysis (DMA). The weight fraction limits for PEG-

and PTMO-based ionenes were 25 and 50 wt%, respectively. Samples with higher soft segment fractions resulted in extremely brittle thin-films with poor mechanical integrity.

DMA was used to characterize the mechanical properties of PTMO25/DD-ionene, PTMO50/DD-ionene, and the PEG25/DD-ionene. As expected, we observed a higher glassy modulus for PTMO50/DD-ionene (750 MPa) when compared to PTMO25/DD-ionene (415 MPa) (**Figure 5a**). This increase in modulus was attributed to a higher weight fraction of soft segment domains in the PTMO50/DD-ionene that can crystallize. The higher crystallinity would lead to an increase in the storage modulus in the glassy plateau.

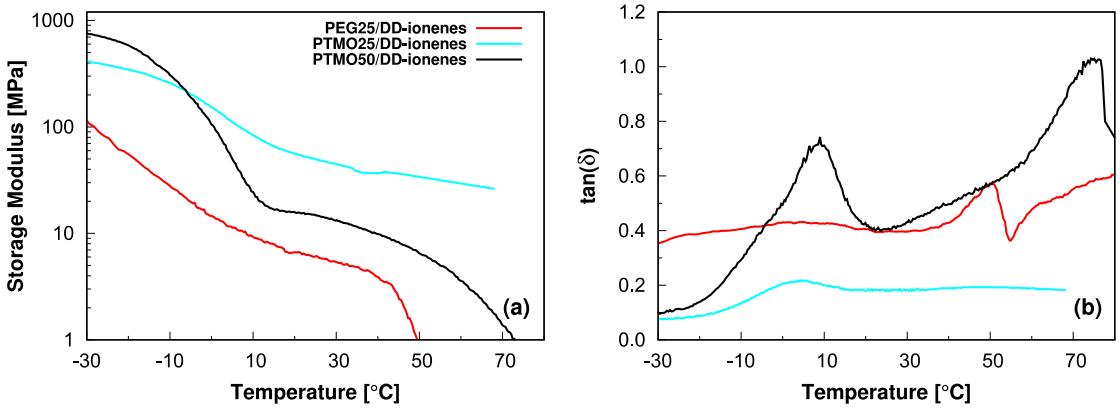

Figure 5: a) Temperature dependence for the storage modulus of the PEG25/DD-ionene, PTMO25/DD-ionene, and PTMO50/DD-ionene and b) Loss factor, tan(δ), of the PEG25/DD-ionene, PTMO25/DD-ionene and PTMO50/DD-ionene.

At approximately -15 ˚C, the storage modulus of PTMO50/DD-ionene starts to decline sharply, followed by a second slower decline starting at approximately 15 ˚C. The first drop in storage modulus is attributed to the melting of the PTMO crystals. The slow decline observed at 15 ˚C is likely due to poor or disordered phase separation that causes the rubbery plateau modulus to slowly decrease. The relatively flatter rubbery

plateaus for the PTMO/DD-ionenes corresponds to the more pronounced hard segment T_gs observed in **Figure 3b**. The melting of the PTMO crystals is also evident from the tan(δ) peak, which is about 5 °C for the PTMO25/DD-ionene and 10 °C for the PTMO50/DD-ionene (**Figure 5b**). The higher intensity of the tan(δ) peak for the PTMO50/DD-ionene reveals the presence of a larger viscous domain compared to the PTMO25/DD-ionene. This verifies that a larger soft segment content participates in the transition and a lower ion content is present in the structure of PTMO50/DD-ionene. The second tan(δ) peak for PTMO50/DD-ionene shows a peak at approximately 70 ˚C and is due to the viscous flow in the hard segments. This is sometimes attributed to ion dissociation and sometimes to segmental mobility. The second tan(δ) peak for the PTMO25/DD-ionene is anticipated around 120 ˚C; which was not measured.

Contrary to PTMO50/DD-ionene, PTMO25/DD-ionene exhibits a linear rubbery plateau beyond the initial drop of storage modulus that persists over a wide range of temperatures (20 – 70 ˚C). This is characteristic of microphase separated morphologies and it is caused by the higher ionic interactions in the ionene with higher fractions of hard segments. Ionic aggregates can be considered to act similar to reversible crosslinks, creating connections between soft segments in the structure, therefore the PTMO25/DD-ionene has the most prolonged rubbery plateau modulus.

The MD simulation results discussed below confirm that the PTMO25/DD-ionene system shows relatively strong microphase separation behavior and the strongest ionic aggregation behavior of all simulated ionenes in the series. Specifically, snapshots show the PTMO25/DD-ionene's aggregates are approximately two ions wide, while the

aggregates are not as thick or as clearly defined in the lower ion content PTMO50/DD-ionene system; more quantitatively, the ionic aggregation can be assessed via the ion-ion pair correlation functions and structure factors, which are also discussed below. Microphase segregation of hard and soft segments is assessed via the PTMO-PTMO and PE-PE structure factors, which show a higher peak at low wavevector for the PTMO25/DD-ionene, corresponding to an increased degree of microphase segregation relative to the PTMO50/DD-ionene.

The storage modulus of the ionene decreased markedly by replacing the PTMO soft segment with PEG at the same molecular weight and weight fraction. The resulting PEG25/DD-ionene is brittle and not suitable for DMA at temperatures lower than -30 ˚C. This difference in elasticity may be connected to the amount of ionic aggregation (which is higher in the PTMOYY/DD-ionene system) because ionic aggregates are known to act similarly to temporary crosslinks in ionomeric systems, increasing the modulus.[22] However, it should be noted that the level of effective crosslinking provided by ionic aggregates in these relatively softer, higher dielectric constant ionenes is relatively modest compared to that present in many ionomers.

For PEG25/DD-ionene, an indistinct tan(δ) peak can be seen at about 0 °C related to soft segment domains. There is also another peak that starts at approximately 40 ˚C and reaches a maximum at approximately 50 ˚C. This indicates that the melting transition of the soft segment in the ionene occurs at a slightly higher temperature than what was measured by DSC (32 ˚C). The next tan(δ) peak, evident at 80 C, originates from a glass transition in the hard segment microdomain, and is consistent with DSC

results which suggest that the PEG25/DD-ionene system has distinct glass transition temperatures for the soft and hard microdomains.

It is worth noting that the elastic modulus increased in the rubbery plateau regime as the PTMO content decreased, which implies the effect of ionic segment association and higher ion content on the thermomechanical properties. At ambient temperature the storage modulus is about 50 MPa and 15 MPa for PTMO25/DD and PTMO50/DD, respectively. Though the modulus was not measured in the current simulations, prior coarse-grained simulations of ionomers observed a similar trend that increasing the fraction of ions increased the modulus (though that work used a lower background dielectric constant and stronger overall ionic aggregation than the simulations presented here).[23] Changing the soft segment to PEG caused a significant decrease in storage modulus at room temperature for the same fraction of soft segment (25 wt%) compared to the PTMO/DD ionenes. The lower elastic modulus of PEG25/DD (about 5 MPa) in the rubbery regime is indicative of a reduction in ionic aggregation in the PEG series compared to the PTMO series.

Simulation Results and Discussion

Microphase Separation

Coarse-grained simulations of PEGXX/DD-ionenes and PTMOYY/DD-ionenes were performed for 3 soft segment weight fractions (25, 50, and 75 wt %). We analyze structure by calculating pair correlation functions, $g_{PE-PE}(r)$ and $g_{PE-PEG}(r)$. These functions show the normalized probability of finding a PE or PEG bead, respectively, as a function of distance from a PE bead. The monomer-scale packing (σ-scale fluctuations starting at the contact distance σ, where σ is the monomer diameter)

typical of polymer melts is clearly seen, and the first peak in $g_{PE-PE}(r)$ is significantly higher than that of $g_{PE-PEG}(r)$, indicating the preference for PE beads to contact each other rather than PEG. Smaller fluctuations that persist to longer distances are also observed at a length scale of $\approx 4\sigma$; this shows that alternating regions exist where PE monomer density is above and below average (and PEG density is below/above average). This feature is most prominent in the PEG25/DD-ionene (**Figure 6a**), is present to a lesser extent in the PEG50/DD-ionene (**Figure 6b**), and is present only relatively locally for the PEG75/DD-ionene (**Figure 6c**). The extent of microphase segregation is more clearly seen in the partial structure factors of the two monomer types, $S_{PE-PE}(k)$ and $S_{PEG-PEG}(k)$, presented in **Figure 7**, where a peak exists at $k \approx \frac{2\pi}{4\sigma}$ corresponding to the longer length scale fluctuations in g(r). This peak's intensity decreases with increasing weight fraction corresponding to less microphase segregation. The peak intensities are modest, and there are no higher order peaks in $S_{PE-PE}(k)$ corresponding to this length scale (and only a small secondary peak in $S_{PEG-PEG}(k)$ exists); this indicates a lack of longer-ranged microphase separated order. Note that the higher wavenumber peak, near $k \approx \frac{2\pi}{\sigma}$, corresponds to typical monomer-scale packing. The relatively local microphase segregation present in these systems, especially at low soft segment fraction, can also be observed in the simulation snapshots of **Figure 10a** and **Figure 10b**.

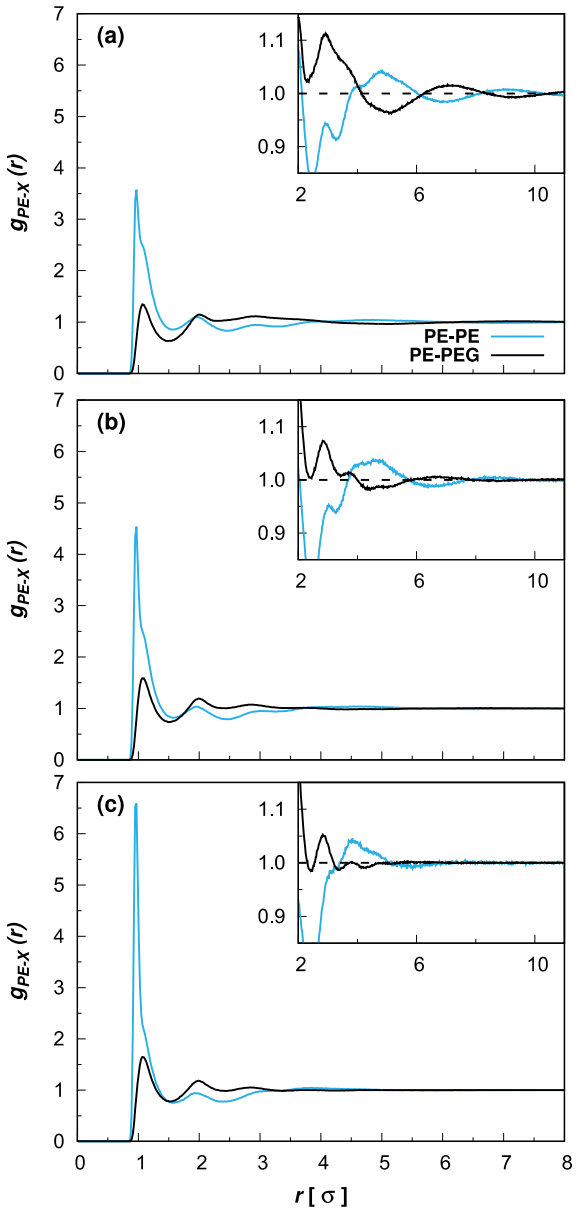

Figure 6: PE-PE and PE-PEG radial distribution functions for (a) PEG25/DD-ionene, (b) PEG50/DD-ionene, and (c) PEG75/DD-ionene. The inset figure shows a smaller region of the same functions.

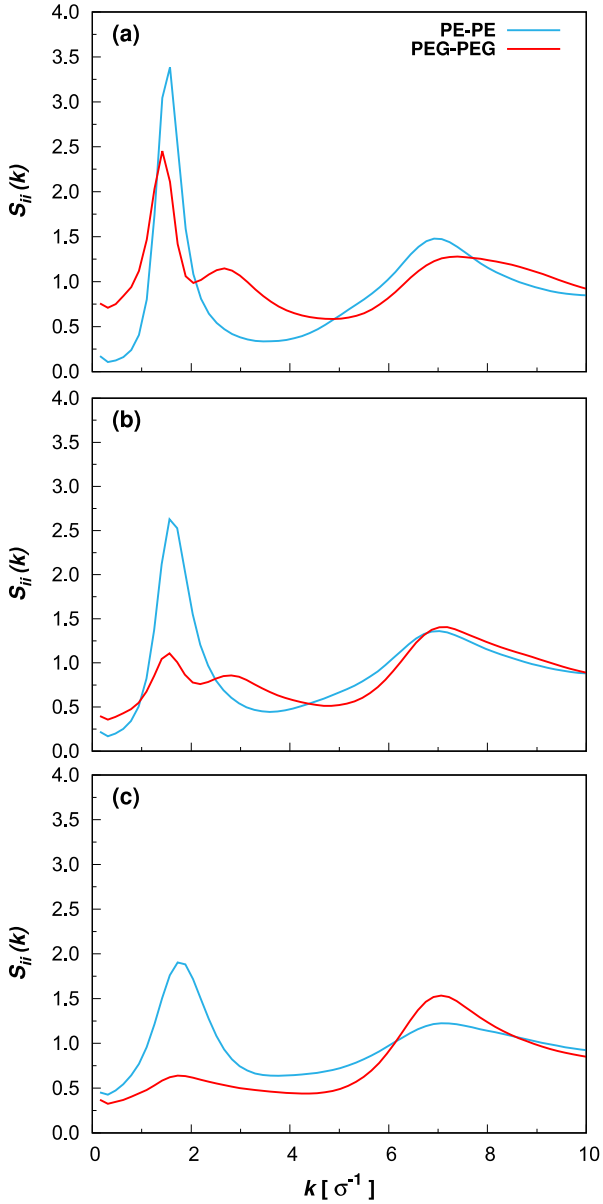

Figure 7: PE-PE and PEG-PEG partial structure factors for (a) PEG25/DD-ionene, (b) PEG50/DD-ionene, and (c) PEG75/DD-ionene.

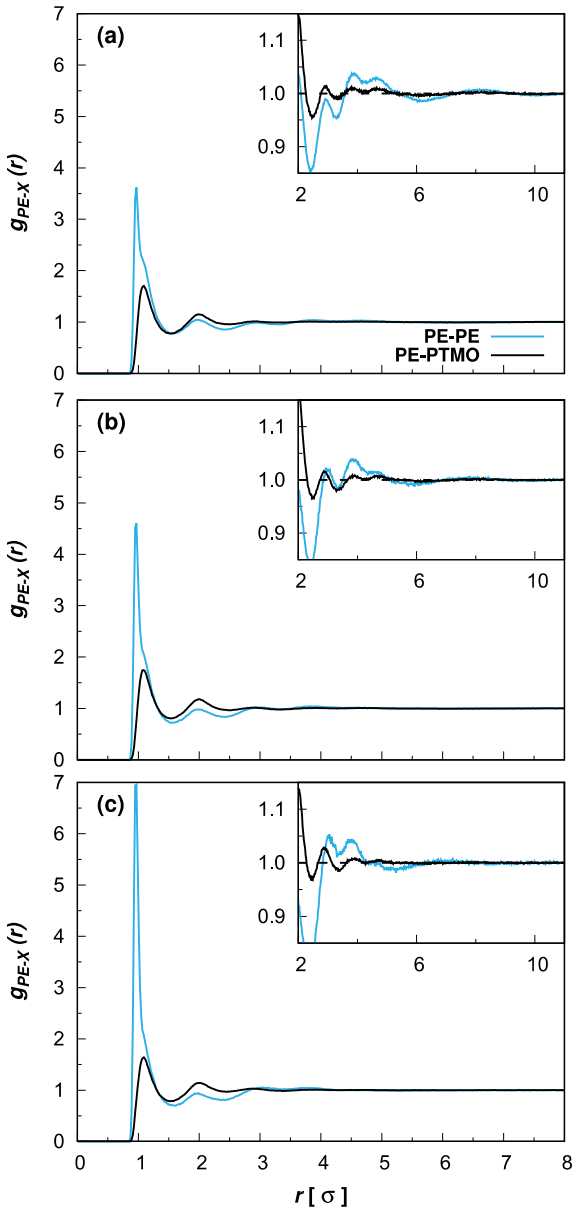

Figure 8: PE-PE and PE-PTMO radial distribution functions for (a) PTMO25/DD-ionene, (b) PTMO50/DD-ionene, and (c) PTMO75/DD-ionene. The inset figure shows a smaller region of the same functions.

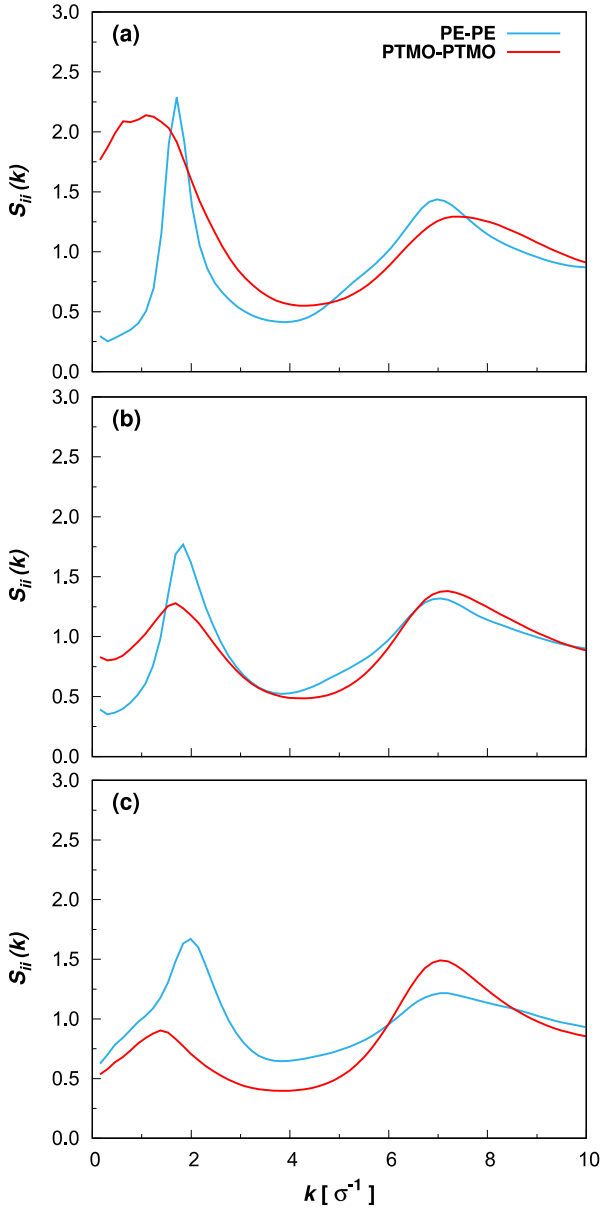

Figure 9: PE-PE and PTMO-PTMO partial structure factors for (a) PTMO25/DD-ionene, (b) PTMO50/DD-ionene, and (c) PTMO75/DD-ionene.

Similar results can be seen for the PTMO-based ionenes, with a preference for PE-PE versus PE-PTMO interactions at contact and alternating fluctuations in PE and PTMO density visible in the pair correlation functions of **Figure 8a-c**. Corresponding low wavenumber peaks of decreasing intensity with increasing soft segment weight fraction are present in the partial structure factors of **Figure 9a-c**.

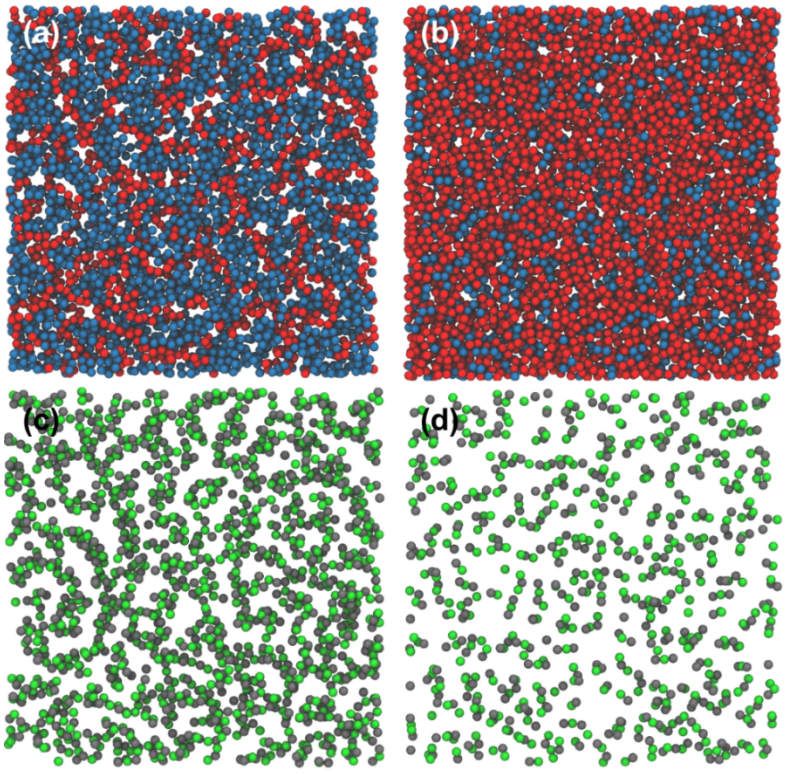

Figure 10: Simulation snapshots of a cross-section (4σ width) of (a and c) PEG25/DD-ionene and (b and d) PEG75/DD-ionene. (a) and (b) show only neutral beads (PE and PEG), with charged beads made invisible. (c) and (d) show only charged beads (ammonium groups and Br^-). PEG beads are red, PE beads are blue, ammonium beads are grey, and Br^- are green.

Ionic Aggregation

To understand ionic aggregation behavior, we also calculate the ion-ion radial distribution function $g_{ion-ion}(r)$, considering average correlations between an ion of either type and any other ion. The average number of ion neighbors $N_{neigh}(r)$ of any ion within a radial distance r is then calculated.

$$N_{neigh} = \int_0^r dr 4\pi r^2 \, \rho_{ion} \, g_{ion-ion}(r), \qquad \text{Equation 1}$$

where ρ_{ion} is the average number density of ions. As seen in **Figure 11**, there is always a strong peak in $g_{ion-ion}(r)$ at contact. The PTMOYY/DD-ionenes (**Figure 11b**) have a more intense first peak and shoulder corresponding to greater ionic aggregation

versus the PEGXX/DD-ionenes (**Figure 11a**), and they also show longer length scale ion density fluctuations (a decrease after the initial peaks then a smaller peak at $\approx 4\sigma$). The differences in these normalized density fluctuations as a function of weight fraction are relatively small, but it is seen that increasing the soft segment content slightly increases ion aggregation and longer range density fluctuation; this is especially noticeable in the range of $\approx \sqrt{2}\sigma$ which is the next nearest neighbor distance between two ions if four ions are packed at contact in a square arrangement. The decreased ionic aggregation for higher soft segment fractions and for PEG versus PTMO systems is likely because increasing the fraction of the more polar PEG segments increases the average dielectric constant in our model (which decreases the strength of ion-ion interactions). Moreover, switching from PTMO to PEG increases the PEG fraction (and dielectric constant) because we model PTMO as a mixture of PE and PEG beads. Also, the calculation of $N_{neigh}(r)$ shows that the number of ions contained within the first neighbor peak and shoulder depends significantly on the soft segment content (or ion concentration). In addition to the small decrease in ionic aggregation with increased soft segment content generally, this is because lower soft segment content also implies higher ion concentration in these systems, which naturally leads to more ion neighbors.

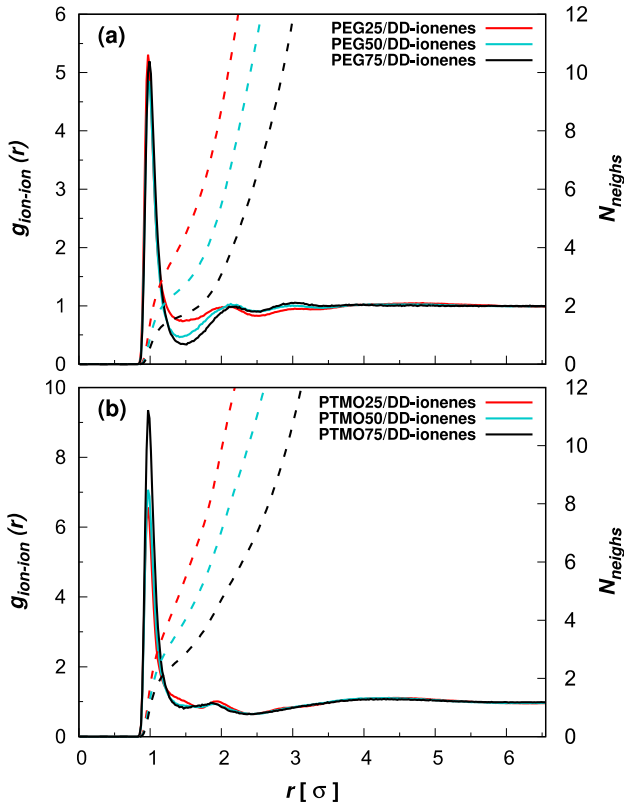

Figure 11: Ion-ion radial distribution functions ($g_{ion-ion}(r)$, solid lines) for 25, 50, and 75 wt % (a) PEG-based and (b) PTMO-based ionenes. Dashed lines indicate the number of ion neighbors, N_{neighs}, a given ion has within sphere of radius r.

The local morphology of ionic aggregation also changes as a function of soft segment weight fraction and soft segment type, as is noticeable in the snapshots of **Figure 10 and Figure 12**. **Figure S3** in the Supporting Information shows additional snapshots, for the PEG50/DD-ionene and the PTMO50/DD-ionene. The most strongly aggregated system considered, PTMO25/DD-ionene, show extended, stringy aggregates that are about two ions wide (see **Figure 12c**). This behavior is consistent with what has been previously reported from coarse-grained simulations of ionenes with a single backbone chemical type at relatively low ϵ_r.[16,17] As dielectric constant increases, either due to switching to PEG segments or increasing soft segment content, the aggregates break into smaller and less well ordered structures, as has been

previously observed for coarse-grained ionenes.[16,17]

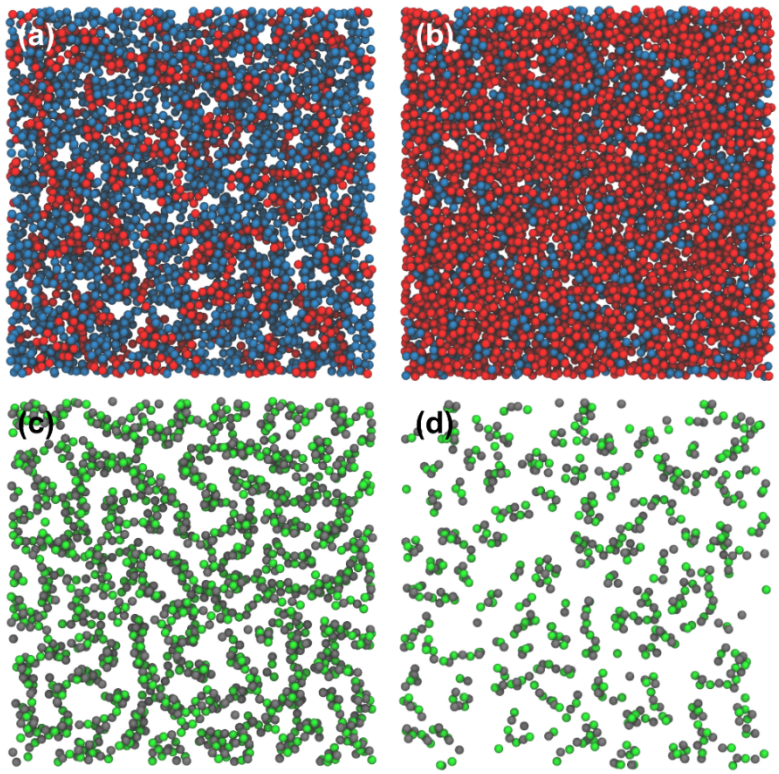

Figure 12: Simulation snapshots of a cross-section (4σ width) of PTMO-based ionene systems at (a and c) 25 wt % PTMO and (b and d) 75 wt % PTMO. (a) and (b) show only neutral beads (PE and PTMO), with charged beads made invisible. (c) and (d) show only charged beads (ammonium groups and Br^-). Beads belonging to PTMO are red (PTMO is composed of a mixture of PEG-type and PE-type beads), PE beads are blue, ammonium beads are grey, and Br^- are green.

Dynamics

The DSC experiments presented above (**Figure 3(e)**) showed two distinct T_g values for the PEG/DD-ionenes, corresponding to the hard and soft microphases (the PTMO/DD-ionenes' soft segment T_g was apparently below the available temperature range). The experimentally measured T_g is related to the temperature at which the repeat unit-scale relaxation time diverges (or, practically, crosses some large value); such relaxation times are straightforward to calculate from simulations, and at a given T above T_g (such as in our simulation), regions of the material that are further from their

local T_g generally have faster relaxation.[24] Thus, though we did not cool the simulated samples to measure T_g, the calculated repeating unit relaxation times of soft and hard segments from simulation can be qualitatively compared with experiments in terms of a) whether the microphases have significantly different dynamics (different relaxation times, different T_gs) and b) which phase and which compositions have faster dynamics (smaller relaxation time, lower T_g). Simulations further allow us to investigate the relative dynamics of the components whose T_g is outside of the experimental measurement. In particular, we probed mobility of a given type of bead by calculating the self-intermediate structure factor,

$$F_s(k,t) = \langle e^{-i\mathbf{k}\cdot[\mathbf{r_j}(t+t_o)-\mathbf{r_j}(t_o)]} \rangle \qquad \text{Equation 2}$$

where the average is taken over all beads j of the given type, over multiple initial reference times t_o, and over multiple wavevectors **k** at the same wavenumber k=|**k**|. Specifically, to consider repeat unit-scale relaxation of soft beads (or hard beads), we calculate $F_s(k_m,t)$ considering only PEG/PTMO (or PE and ion-type) beads at $k_m = 2\pi/\sigma$. As a measure of relaxation time, we report the value of t at which F_s has decayed to $1/e$ (denoted by τ_m); this value is identified by interpolating $F_s(k_m,t)$ based on a stretched exponential form.

$F_s(k_m,t)$ for PEG in the PEGXX/DD-ionene systems can be seen in **Figure 13(a)**; the curves decay more quickly, corresponding to decreasing τ_m in **Figure 13(b)** and indicating faster segmental relaxation, as the weight fraction of PEG increases. This result is consistent with the experimental trend that soft segment T_g decreases with increasing weight fraction, validating that our coarse-grained model is reproducing a

major aspect of the mobility of these systems.

The trend in hard segment mobility (considering both PE and ions together) is similar to that of soft segment mobility in PEGDD/ionenes; relaxation times decrease with an increasing weight fraction of PEG. Further calculations of the repeating unit relaxation times for ionic beads alone (not shown) suggest that the mobility of ionic beads is also reduced in the lower weight fraction systems. Thus, the increased microphase segregation and ionic aggregation observed in the ionenes with lower weight fractions of soft segment coincide with decreased soft segment, hard segment, and ionic mobility.

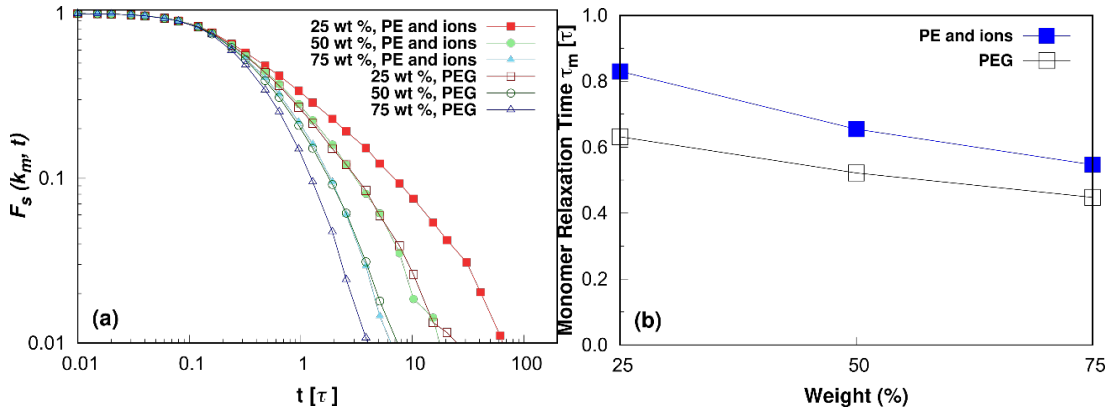

Figure 13: (a) Self-intermediate structure factor for soft segments (open symbols) and hard segments (closed symbols, PE and ionic beads) at the labeled weight fractions and with $k_m = 2\pi/\sigma$. (b) Corresponding repeating unit relaxation times (τ_m) of the soft segment (PEG) and hard segment (PE and ions) mobility at varying soft segment weight fractions. Results are block averaged over 3 time windows; considering the time windows separately, the standard deviation in τ_m is between 0.002 and 0.005τ for PEG, and between 0.008 and 0.02τ for PE and the ions.

While experimental measurements of the soft segment T_gs of PTMO/DD-ionenes are not available, we also calculated $F_s(k_m, t)$ and τ_m for hard and soft segments of this series (see **Figure 14**). Analogous to the results of the PEG series, both soft (PTMO) and hard segment relaxation times decrease as the PTMO weight fraction increases, suggesting increased mobility with increasing soft weight fraction.

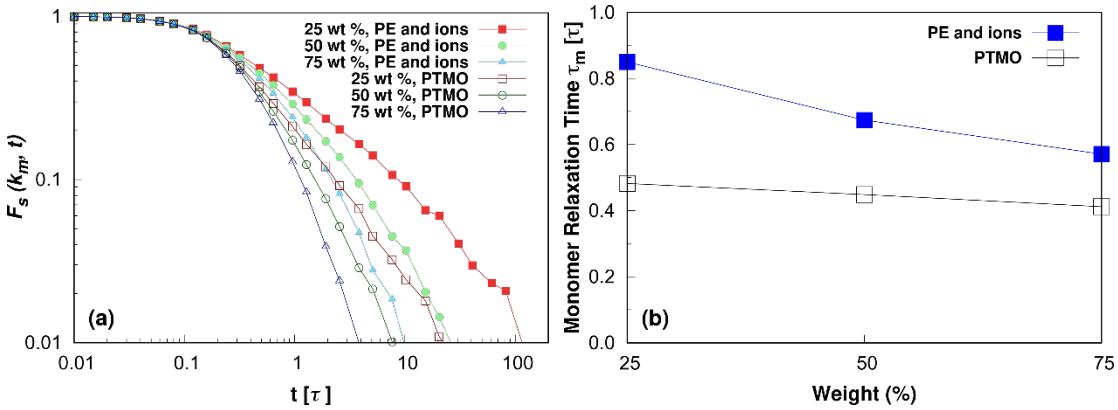

Figure 14: (a) Self-intermediate structure factor for PTMO (open symbols), and for a combination of all PE and ionic beads (closed symbols). (b) Repeating unit relaxation times (τ_m) of the soft segment (PTMO) and hard segment (PE and ions) mobility at varying soft segment weight fraction. Results are block averaged over 3 time windows; considering the time windows separately, the standard deviation in τ_m is between 0.002 and 0.005τ for PTMO, and between 0.004 and 0.01τ for PE and the ions.

Thus, if soft segment T_g were measured experimentally, we would predict it to decrease at higher PTMO weight fractions. When comparing the PTMO and PEG series data to each other, the simulations do seem to capture the relative difference in soft segment mobility between PEG and PTMO. In particular, **Figures 13(b) and 14(b)** shows a clear increase in PTMO soft segment mobility relative to PEG (τ_m is consistently lower in the PTMO/DD-ionene systems). These results are consistent with the soft segment T_g in PTMO being lower than that observed for PEG. There is an inconsistency in the hard segment results in that the hard segment T_g for the PTMO25/DD-ionene system is observed to be significantly higher than that of the PEG25/DD-ionene system in DSC (**Figure 3(e)**), yet simulation results (**Figures 13(b) and 14(b)**) suggest similar hard segment mobility in the PTMO25/DD-ionene relative to the PEG25/DD-ionene. This discrepancy could be due to the difference in measuring ion and PE bead mobility regardless of their location within the structure versus an experimental measure of T_g that corresponds to dynamic arrest of local regions of the

sample (that may include effects of soft segment repeating units mixed into the hard segment regions or exclude effects of some ions or hard segments outside of the regions). It would be of interest to consider a local dynamical analysis in simulation or experimentally determine the hard segment T_g across the entire range of compositions in the future.

Conclusions

A series of random copolymer ionenes were synthesized with varying weight fractions of either 2000 g/mol PTMO or PEG soft segments. An increase in the charge density along the ionene backbone resulted in confinement of the soft segment, leading to a depression in the melting temperature, a reduction in the degree of crystallinity, and in some instances improved elastomeric behavior. This confinement likely arises in part from the presence of ionic aggregates, which act as reversible crosslinks; the level of ionic aggregation was observed to increase as soft segment content decreased in simulation, and when switching the soft segments from PEG to PTMO monomers (which are less polar and have a lower charge screening ability). As expected, increased ionic associations resulted in elastomeric behavior, evidenced by the appearance of a rubbery plateau in the lower weight fraction PTMO-based ionene systems. The experimentally observed trends were connected to simulation results, which showed how changing the type and content of the soft segment spacer influenced microstructure and phase separation. Increasing the charge density (reducing the soft segment content) led to stronger microphase segregation, reduced soft-segment mobility, and an increase in the connectivity and size of the ionic aggregates that formed. Moreover, this

reduction in soft-segment mobility is consistent with the trend in the glass transition temperature with weight fraction observed in DSC. Together, these findings suggest a material with a semi-crystalline and microphase separated morphology, whose structure and phase behavior is strongly influenced by charge density, the degree of ionic aggregation, and the resulting level of confinement and mobility of the soft segments. While only one counterion was studied here, changing counterion type is another avenue to adjust microphase segregation, ionic aggregation, and overall properties that would be of interest to study in future work on these materials. Given the ability to precisely control the soft segment length and weight fraction synthetically, these observations are an important step in establishing a set of design rules for microphase separated elastomers made from segmented ionenes.

Experimental

Materials

2000 g/mol poly(ethylene glycol) (PEG) and poly(tetramethylene oxide) (PTMO) were purchased from Sigma-Aldrich. 6-Bromohexanoyl chloride (97%) was purchased from Alfa Aesar. Triethylamine was purchased from Aldrich and distilled from calcium hydride. 1,12-Dibromododecane (98%) was purchased from Sigma-Aldrich and recrystallized from ethanol. Phenolphthalein and N,N,N',N'-tetramethyl-1,6-hexanediamine (99%) were purchased from Acros Organics and used as received. Methanol (MeOH, HPLC grade) was purchased from Fisher and used as received.

Synthesis of Bromine End-Capped PEG (Br-PEG$_n$-Br) or PTMO (Br-PTMO$_n$-Br)

The reaction was performed according to previous literature precedent.[25,26] The

molecular weight was determined using a combination of alcohol group titration and analysis by ^{1}H NMR spectroscopy. For example, PTMO or PEG 2000 (7.00 g, 3.5 mmol) and TEA (0.79 g, 7.8 mmol) were mixed in dichloromethane (23 mL) at 0 ℃, and 6-bromohexanoyl chloride (1.68 g,7.8 mmol) was added drop-wise. The mixture was slowly warmed to 23 ˚C and stirred for 24 h. Following the reaction, the triethyl-ammonium chloride salt was filtered, and the organic phase was washed with a saturated aqueous solution of sodium bicarbonate and water in series. The organic phase was dried over anhydrous sodium sulfate and removed using rotary evaporation at 23 ˚C. A clear, viscous liquid was obtained.

Synthesis of PEG or PTMO-Based Ionenes with varying soft segment weight ratios

A flame-dried, 50-mL, two-neck, round-bottomed flask was charged Br-PEG$_n$-Br or Br-PTMO$_n$-Br, 1,12-dibromododecane, and N,N,N',N'-Tetramethyl-1,6-hexanediamine. For instance, the PEG25/DD-ionene was prepared by adding 25 wt% of Br-PEG$_n$-Br over the sum of the mass of all three components. The molar ratio of the sum of Br-PEG$_n$-Br or Br-PTMO$_n$-Br and 1,12-dibromododecane to N,N,N',N'-Tetramethyl-1,6-hexanediamine was kept to 1 in all series of ionenes. The example of the actual amount of three components based on the above calculations of PEG25/DD-ionenes is 0.5 g, 0.9607 g, and 0.5389 g for Br-PEG$_n$-Br, 1,12-dibromododecane, and N,N,N',N'-Tetramethyl-1,6-hexanediamine, respectively. The polymerization was performed for 24 h at 75 ℃ in MeOH at 20% weight volume percent. The PEG-based ionene dissolved in MeOH was then cast into films. The slow removal of methanol was required to avoid film defects, so it was allowed to evaporate at room temperature for

3 days. Subsequently, the films were heated in TeflonTM molds at 60 ℃ for 2 days. Finally, the polymer films were dried in vacuo (0.1 mmHg) at 30 ℃ for 24 h. Ionene films were stored in petri dishes containing desiccant and placed in a desiccator until their thermal, mechanical, and morphological properties were measured.

Characterization

^{1}H NMR spectroscopic analyses were performed on Bruker Avance III 500 MHz spectrometer to confirm the monomer and polymer composition at ambient temperature. Differential scanning calorimetry (DSC) was conducted on a TA Instruments Q2000 under a nitrogen flow of 50 mL/min. Samples were first heated from room temperature to 150 ℃ at a heating rate of 10 ℃/min and held at 150 ˚C for 10 min. The cooling rate was 10 ℃/min, and the samples were cooled to -80 ℃ and held there for 10 min, and subsequently were heated to 150 ℃ at the same rate. Thermogravimetric analysis (TGA) was conducted on a TA Instruments Hi-Res TGA 2950 under nitrogen at a heating rate of 10 ℃/min. X-ray Diffraction (XRD) was conducted on a PANalytical X'Pert PRO MRD to confirm the crystalline properties of the segmented ionene copolymers. Dynamic mechanical analysis (DMA) was conducted on a Mettler Toledo Polymer-1 analyzer in a temperature range of -30 to 80 ˚C at a heating rate of 2 ˚C/min, a frequency of 1 Hz, and under 0.1% strain. Due to the hygroscopic nature of ionenes, the samples were heated under vacuum to eliminate moisture before characterization.

Simulation Methodology

Model

Using a coarse-grained molecular model in which each polymer bead represents

three heavy atoms (C, N, or O) and their associated H atoms, we simulate the previously described PEG and PTMO-based dry ionene systems with PE spacers and Br^- counterions (with Br^- each represented as a single coarse-grained bead), as shown conceptually in Figure. This model and our simulation methods are similar to those employed in our prior work on PPG-based ionenes.[14] Our goal is to use a model simple enough to allow for simulations that are tractable to run for much longer than the relaxation time of the chains, while still being detailed enough to show major features of the systems' structure (especially microphase segregation and ionic aggregation, and how these change with soft segment content). We note that our simple model does not include the structural detail of the PEG backbones that would allow them to crystallize like PEG at lower temperatures. Even though varying amounts of crystallinity can be observed in the experimental systems (**Figure 4**), we consider only melt systems in our simulations (without crystallinity), which we run at an increased temperature of $T^*=1.2$ (corresponding to T=360K). This increased temperature also ensures we can fully equilibrate the simulations, as our chain relaxation times are relatively slow at our standard temperature $T^*=1$ (corresponding to 300K).

The model segmented ionene chains are made of alternating uncharged and charged segments; to keep the simulations tractable, we create relatively short chains containing two charged segments with an uncharged segment in between them and on either end. The two end segments are approximately half the length of the middle section, as in prior work.[14] This choice is motivated by the fact that a crucial length scale in ion containing polymers is the spacing between ions along the chain; backbone segments

bridging between two ionic aggregates their ions are participating in, or loops of a backbone segment back into the same aggregate, or tail segments of half the length (that do not loop back into another aggregate because they do not contain an ion on the end), all act to set a similar length scale of order between ionic aggregates.[14,16,17] Moreover, the shorter chains allow us to avoid entanglements, keeping the equilibration times more reasonable.[14]

More specifically, the charged segments consist of two coarse-grained PE beads that each represent (-CH_2-CH_2-CH_2-), with an ammonium group (-$N^+(CH_3)_2$-) on either side, and two Br^- which are added to the system for each charged segment, making the system charge neutral. The uncharged segments are either relatively short polyethylene (PE) segments or longer soft segments composed of PEG or PTMO. Each PEG bead represents (-CH_2-O-CH_2-). Given these chemical units, the masses of the ammonium, PEO, and PE beads are all similar, and these are set to 1 in the reduced mass units of our simulation, corresponding to approximately $44\ \frac{g}{mol}$. The mass of a Br^- bead is then set to 1.82 in reduced units. To keep the model simple and allow for clearer comparisons between PEG and PTMO systems, we represent PTMO using a combination of PEG and PE beads. Specifically, approximating that (-CH_2-CH_2-O-), (-CH_2-O-CH_2-), and (-O-CH_2-CH_2-) can all be represented through the same PEG type of bead, every 3 PTMO chemical monomers can be represented with the bead sequence (-PE-PEG-PE-PEG-PEG-) = $(-CH_2-CH_2-CH_2-CH_2-O-)_3$. The sequence is periodic, and as each segment is created, the number of beads required are selected from the infinitely repeating sequence. In terms of the overall segment architecture, chains are built with uncharged

segment types (PE versus PEG or PTMO) chosen randomly, weighted to yield the appropriate overall fraction of PE to PEG or PTMO segments based on the desired soft segment weight fraction. The soft segment length is 46 beads to approximately represent the experimental soft segments of molecular weight 2k. The approximately half length soft segments at the ends of the chain contain 22 beads rather than 23 because we had performed initial testing on PEG-1K based systems (not shown) which had 23 and 11 beads in the full and half segments, respectively, and we doubled these lengths to quickly compare across these systems. The full resulting architecture is schematically shown in **Figure 13**.

As in prior work, we consider a simple, standard bead-spring model for our chains, but with adjusted intermolecular interaction parameters to approximately capture the chemistry of the system.[14] Specifically, we create our linear chains using finitely extensible (FENE) bonds with standard parameters to prevent chain crossing as in the work of Kremer and Grest.[27,28] All nonbonded bead-bead interactions include the standard 12-6 Lennard-Jones (LJ) potential, shifted and cut off at $r_c = 2.5\sigma$. As is standard practice with FENE bonds, only the repulsive part of the LJ potential (up to $2^{1/6}\,\sigma$) is used between bonded beads. To represent the specific chemical groups present in our system (importantly, we hope to capture the main features that PE and PEG prefer to locally segregate from each other and PEG dissolves ions more easily than PE), we use pairwise interaction parameters as in the Martini 3 model.[29] This model expands on the Martini 2 model[30] that we considered in our prior work,[14] but Martini 3 introduces more granular bead types and increased flexibility in mapping heavy atoms to beads

through the introduction of small (S) and tiny (T) beads, alongside the normal (N) sized beads. The practice of using smaller bead sizes was occasionally found in Martini 2 models,[30–32] but was formalized in Martini 3. Here, we use entirely small bead types such that all beads have the same like-like diameter to simplify local packing behavior. While the results are given in reduced units of σ, to map to real units we use the Martini 3 suggested mapping of small bead diameter σ=0.4 nm.

The details of how the specific Martini 3 types were chosen based on the chemical groups represented by each bead, along with all interaction parameters, are given in the Supporting Information. Briefly, Martini includes charged (Q), polar (P), nonpolar (N), and apolar (C) types, along with hydrogen bond acceptor (a) and donor (d) subtypes, and specific interaction levels which can be selected based on the level of polarity or other considerations. Martini 3 usually includes several suggestions for mappings to atomic structure for each bead type. Here, we choose types SN1a for PEG, SC2 for PE, SQ0 for C_2N^+, and SQ1 for Br^-; the ionic beads are chosen to match the building blocks in the PPG-based ammonium ionene model from the literature.[14] The PE and PEG parameters are chosen considering that 1. The corresponding homopolymers should be harder and softer, respectively (PE-PE interactions should be stronger than PEG-PEG interactions), 2. the PEG-PEG and PE-PE like interactions are more favorable than the PE-PEG cross interactions; and 3. the ions are better solvated by PEG versus PE. One effect of this choice is that Br^- is mapped to 1 heavy atom/bead, whereas 3 heavy atoms/bead are used for PEO, PE, and C_2N^+. This breaks with the standard Martini 3 recommendation which would typically use a tiny bead for a single atom. Note also

that, while all like interactions use the same bead diameter, the cross-interaction of the most hydrophobic type (C2) with the ionic types (SQ0 and SQ1) has a longer range based on the Martini parameters for these types, which were chosen to allow ionic beads to retain their solvation shell when pulled into an apolar medium.[30]

Charges are assigned such that cations and anions have charge $\pm e$, and all other beads have zero charge; ions interact via the Coulomb potential. Unlike more detailed atomistic models, there are no partial charges, nor accounting for induced dipole-based interactions (as in polarizable models). Consequently, we set the background dielectric constant ϵ_r to approximately capture the charge screening behavior of the medium, which includes the more polar PEG monomers, PE monomers, and ionic species (whose polarizability is relevant but whose charges are already explicitly represented and need not be accounted for by the background ϵ_r). This strategy is typical in coarse-grained ionene and ionomer models in the literature.[14,16,17] Here, ϵ_r is calculated using a bead number density weighted average of the approximate dielectric constants of PE ($\epsilon_r = 2$) and PEG ($\epsilon_r = 8$), and including ions at the same value as PE ($\epsilon_r = 2$) for simplicity and due to their relatively low average polarizability.[14] Exact ϵ_r values for each system are provided in the Supporting Information. Long-range Coulombic interactions are calculated using the P^{3}M method with a relative error of 10^{-4}.

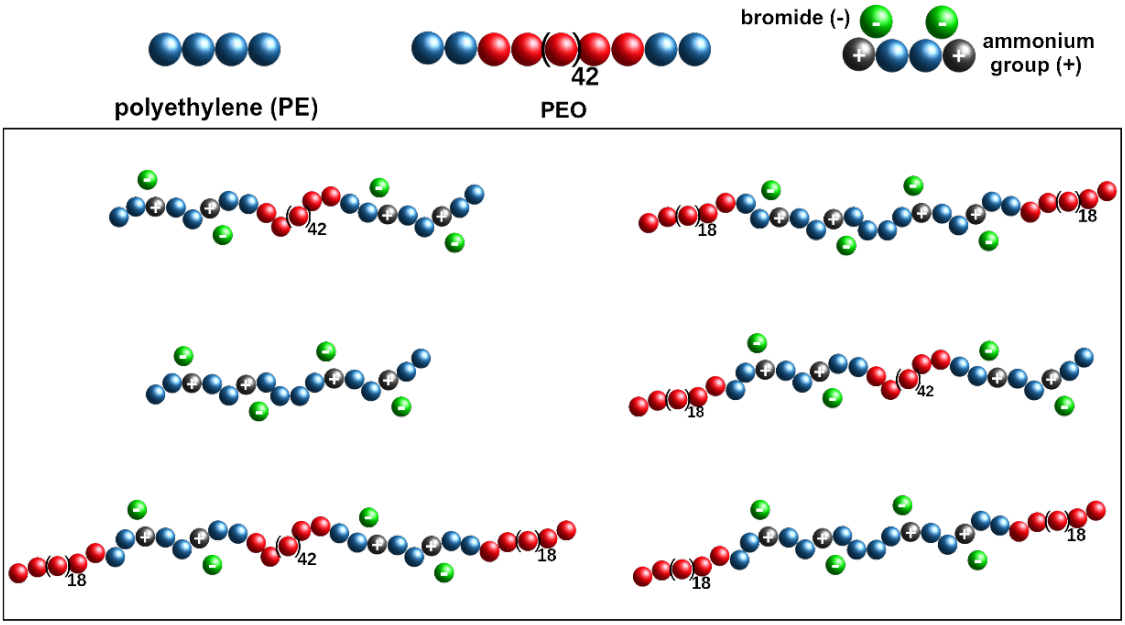

Figure 15: Schematic of coarse-grained segment types (top), and all possible chains which are formed using these three segments (bottom) for PEO-based ionenes. Ammonium beads (-$N(CH_3)_2^+$-) are in black, Br^- are in green, PE beads (-CH_2- CH_2-CH_2-) are in blue, and PEG beads (-CH_2-O-CH_2-) are in red, except the latter two implicitly end in CH_3 when at the end of chains. PTMO-based ionenes include the same bead types and overall chain structure, but the PTMO segments have a mixture of PEO and PE beads as described in the text.

Simulation Details

The MD software LAMMPS[33,34] was used to run all simulations. Long-range coulombic interactions are calculated using the particle-particle particle-mesh algorithm.[35]

We create PEG/DD-ionene and PTMO/DD-ionene systems at 25, 50, and 75 soft wt % (the specific definition of soft weight fraction for our model is analogous to the experimental definition and is given in the Supporting Information) with system sizes of 2000, 1500, and 900 chains, respectively, resulting in box lengths of $\approx 40\sigma$. From an initial state of random walk chains, we perform brief pushoff and minimization runs in order to remove bead overlaps, followed by NPT equilibration at the desired

temperature ($T^* = 1.2$) and pressure (P^*=0) for $2 \cdot 10^5\tau$ using velocity Verlet integration, a timestep of $\Delta t = 0.005$, and a Nose-Hoover thermostat and barostat. Time constants of 1τ and 5τ are used for the thermostat and barostat, respectively. Further details of our initialization and equilibration procedure can be found in the Supporting Information.

Prior to data collection, the simulation was equilibrated for an additional $5 \cdot 10^4\tau$ (10 million steps) in the NVT ensemble before data collection, using a Nosé-Hoover thermostat at temperature $T^* = 1.2$ as in the data collection run. It should be noted that the total equilibration time between NPT and NVT is $2.5 \cdot 10^5\tau$, which is $\gtrapprox$ 10 times that required for the end-to-end vector ACF to decay to $1/e$; details can be found in the Supporting Information.[17,36] When switching from NPT to NVT, an average box length (L) was calculated based on a short (500τ) run and a step with an L-value nearly equal to L_{avg} was selected (matching up to the hundredths place to L_{avg}) to start the NVT run. The data collection NVT run was performed over a period of $15 \cdot 10^3\tau$, during which coordinates were saved every $250\,\tau$. Pair correlation functions $g(r)$ are calculated from these snapshots using VMD.[37] Following Ref. [38], $S(k)$ is calculated by adding 1 to the Fourier transform of the product of $h(r) = g(r) - 1$ and a window function meant to reduce artifacts due to the finite cutoff used in the integral.[38] Further details on the calculation of $g(r)$ and $S(k)$ can be found in the Supporting Information.

Author contributions

Nicholas Liesen: Conceptualization, investigation, writing – original draft, and writing

– review & editing. Meng Wang: Conceptualization, investigation, writing – original draft and writing – review & editing. Mehrnoosh Taghavimehr: Conceptualization, investigation, writing – original draft, and writing – review & editing. Jae Sang Lee: Investigation, writing – original draft, and writing – review & editing. Reza Montazami: Conceptualization, investigation, project administration, supervision, visualization, funding acquisition, writing – original draft, and writing – review & editing. Lisa M. Hall: Conceptualization, investigation, project administration, supervision, visualization, funding acquisition, writing – original draft, and writing – review & editing. Matthew D. Green: Conceptualization, investigation, project administration, supervision, visualization, funding acquisition, writing – original draft, and writing – review & editing.

Conflicts of interest

There are no conflicts to declare.

Acknowledgments

This work was financially supported in part by the Army Research Office (W911NF-18-1-0412) and NASA (80NSSC18K1508). Also, the authors acknowledge the Ohio Supercomputer Center for computing time.

Supporting Information

Additional details and discussion of the MD simulations, supplemental NMR spectra, raw XRD traces.

References

(1) Yang, Y.; Urban, M. W. Self-Healing of Polymers via Supramolecular Chemistry. *Adv. Mater. Interfaces* **2018**, *5* (17), 1–19. https://doi.org/10.1002/admi.201800384.

(2) Leir, C. M.; Stark, J. E. Ionene Elastomers from Polytetramethylene Oxide Diamines and Reactive Dihalides. I. Effect of Dihalide Structure on Polymerization and Thermal Reversibility. *J. Appl. Polym. Sci.* **1989**, *38* (8), 1535–1547. https://doi.org/10.1002/app.1989.070380810.

(3) Feng, D.; Venkateshwaran, L. N.; Wilkes, G. L.; Leir, C. M.; Stark, J. E. Structure-Property Behavior of Elastomeric Segmented PTMO–Ionene Polymers. II. *J. Appl. Polym. Sci.* **1989**, *38* (8), 1549–1565. https://doi.org/10.1002/app.1989.070380811.

(4) Feng, D.; Wilkes, G. L.; Leir, C. M.; Stark, J. E. Morphological Investigation of Polytetba-Methyleneoxide-Dibbomoxylene Segmented Ionene Polymebs by Tbansmission Electbon Micboscopy and Small-Angle X-Ray Scattebing. *J. Macromol. Sci. Part A - Chem.* **1989**, *26* (8), 1151–1181. https://doi.org/10.1080/00222338908052040.

(5) Lee, J. S.; Hocken, A.; Green, M. D. Advances in the Molecular Design of Ionenes for a Diverse Range of Applications. *Mol. Syst. Des. Eng.* **2021**, Advance Article. https://doi.org/10.1039/D1ME00007A.

(6) Loveday, D.; Wilkes, G. L.; Bheda, M. C.; Shen, Y. X.; Gibson, H. W. Structure-Property Relationships in Segmented Polyviologen Ionene Rotaxanes. *J. Macromol. Sci. Part A* **1995**, *32* (1), 1–27. https://doi.org/10.1080/10601329508011061.

(7) Ikeda, Y.; Yamato, J.; Murakami, T.; Kajiwara, K. Aliphatic Poly(Oxytetramethylene) Ionenes: Effect of Counter-Anion on the Properties and Morphology. *Polymer (Guildf).* **2004**, *45* (25), 8367–8375. https://doi.org/10.1016/j.polymer.2004.09.082.

(8) Klun, T. P.; Wendling, L. A.; Van Bogart, J. W. C.; Robbins, A. F. Structure–Property Relationships of Ionene Polymers. *J. Polym. Sci. Part A Polym. Chem.* **1987**, *25* (1), 87–109. https://doi.org/10.1002/pola.1987.080250109.

(9) Williams, S. R.; Long, T. E. Recent Advances in the Synthesis and Structure–Property Relationships of Ammonium Ionenes. *Prog. Polym. Sci.* **2009**, *34* (8), 762–782. https://doi.org/10.1016/j.progpolymsci.2009.04.004.

(10) Liu, S.; Ono, R. J.; Wu, H.; Yng, J.; Chang, Z.; Xu, K.; Zhang, M.; Zhong, G.; Tan, J. P. K.; Ng, M.; Yang, C.; Chan, J.; Ji, Z.; Bao, C.; Kumar, K.; Gao, S.; Lee, A.; Fevre, M.; Dong, H.; Ying, J. Y.; Li, L.; Fan, W.; Hedrick, J. L.; Yan, Y. Biomaterials Highly Potent Antimicrobial Polyionenes with Rapid Killing Kinetics , Skin Biocompatibility and in Vivo Bactericidal Activity. *Biomaterials* **2017**, *127*, 36–48. https://doi.org/10.1016/j.biomaterials.2017.02.027.

(11) Petersen, H.; Fechner, P. M.; Martin, A. L.; Kunath, K.; Stolnik, S.; Roberts, C. J.; Fischer, D.; Davies, M. C.; Kissel, T. Polyethylenimine-Graft-Poly(Ethylene Glycol) Copolymers: Influence of Copolymer Block Structure on DNA

Complexation and Biological Activities as Gene Delivery System. *Bioconjug. Chem.* **2002**, *13* (4), 845–854. https://doi.org/10.1021/bc025529v.

(12) Burmistr, M. V.; Sukhyy, K. M.; Shilov, V. V.; Pissis, P.; Polizos, G.; Spanoudaki, A.; Gomza, Y. P. Structure, Thermal Properties and Ionic Conductivity of Polymeric Quaternary Ammonium Salts (Polyionenes) Containing Ethylene Oxide and Aliphatic Chain Fragments. *Solid State Ionics* **2005**, *176* (19–22), 1787–1792. https://doi.org/10.1016/j.ssi.2005.04.032.

(13) Thankamony, R. L.; Chu, H.; Lim, S.; Yim, T.; Kim, Y.-J.; Kim, T.-H. Preparation and Characterization of Imidazolium-PEO-Based Ionene/PVDF(HFP)/LiTFSI as a Novel Gel Polymer Electrolyte. *Macromol. Res.* **2015**, *23* (1), 38–44. https://doi.org/10.1007/s13233-015-3001-9.

(14) Vijayaraghavan, P.; Brown, J. R.; Hall, L. M. Modeling the Effect of Polymer Composition on Ionic Aggregation in Poly(Propylene Glycol)-Based Ionenes. *Macromol. Chem. Phys.* **2016**, *217* (8), 930–939. https://doi.org/10.1002/macp.201500466.

(15) Wong, C.; Clarke, J. H. R. Molecular Dynamics Simulation of Microstructure and Counterion Transport in Dry Ionic Heteropolymers. *J. Chem. Phys.* **2002**, *116* (15), 6795–6802. https://doi.org/10.1063/1.1461356.

(16) Hall, L. M.; Stevens, M. J.; Frischknecht, A. L. Effect of Polymer Architecture and Ionic Aggregation on the Scattering Peak in Model Ionomers. *Phys. Rev. Lett.* **2011**, *106* (12), 127801. https://doi.org/10.1103/PhysRevLett.106.127801.

(17) Hall, L. M.; Seitz, M. E.; Winey, K. I.; Opper, K. L.; Wagener, K. B.; Stevens, M. J.; Frischknecht, A. L. Ionic Aggregate Structure in Ionomer Melts: Effect of Molecular Architecture on Aggregates and the Ionomer Peak. *J. Am. Chem. Soc.* **2012**, *134* (1), 574–587. https://doi.org/10.1021/ja209142b.

(18) Buitrago, C. F.; Bolintineanu, D. S.; Seitz, M. E.; Opper, K. L.; Wagener, K. B.; Stevens, M. J.; Frischknecht, A. L.; Winey, K. I. Direct Comparisons of X-Ray Scattering and Atomistic Molecular Dynamics Simulations for Precise Acid Copolymers and Ionomers. *Macromolecules* **2015**, *48* (4), 1210–1220. https://doi.org/10.1021/ma5022117.

(19) Sampath, J.; Hall, L. M. Impact of Ionic Aggregate Structure on Ionomer Mechanical Properties from Coarse-Grained Molecular Dynamics Simulations. *J. Chem. Phys.* **2017**, *147* (13), 134901. https://doi.org/10.1063/1.4985904.

(20) Ruckenstein, E.; Chen, X. Covalent Cross-Linking of Polymers through Ionene Formation and Their Thermal De-Cross-Linking. *Macromolecules* **2000**, *33* (24), 8992–9001. https://doi.org/10.1021/ma0006272.

(21) Tsutsui, T.; Tanaka, R.; Tanaka, T. Mechanical Relaxations in Some Ionene Polymers. I. Effect of Ion Concentration. *J. Polym. Sci. Polym. Phys. Ed.* **1976**, *14* (12), 2259–2271. https://doi.org/10.1002/pol.1976.180141211.

(22) Pineri, M.; Eisenberg, A. *Structure and Properties of Ionomers*; Springer Science & Business Media, 2012; Vol. 198.

(23) Sampath, J.; Hall, L. M. Impact of Ion Content and Electric Field on Mechanical Properties of Coarse-Grained Ionomers. *J. Chem. Phys.* **2018**, *149* (16), 163313.

(24) Mangalara, J. H.; Mackura, M. E.; Marvin, M. D.; Simmons, D. S. The

Relationship between Dynamic and Pseudo-Thermodynamic Measures of the Glass Transition Temperature in Nanostructured Materials. *J. Chem. Phys.* **2017**, *146* (20), 203316.

(25) Tamami, M.; Williams, S. R.; Park, J. K.; Moore, R. B.; Long, T. E. Poly(Propylene Glycol)-Based Ammonium Ionenes as Segmented Ion-Containing Block Copolymers. *J. Polym. Sci. Part A Polym. Chem.* **2010**, *48* (19), 4159–4167. https://doi.org/10.1002/pola.24186.

(26) Williams, S. R.; Salas-de la Cruz, D.; Winey, K. I.; Long, T. E. Ionene Segmented Block Copolymers Containing Imidazolium Cations: Structure–Property Relationships as a Function of Hard Segment Content. *Polymer (Guildf).* **2010**, *51* (6), 1252–1257. https://doi.org/10.1016/j.polymer.2009.06.051.

(27) Grest, G. S.; Kremer, K. Molecular Dynamics Simulation for Polymers in the Presence of a Heat Bath. *Phys. Rev. A* **1986**, *33* (5). https://doi.org/10.1103/PhysRevA.33.3628.

(28) Kremer, K.; Grest, G. S. Dynamics of Entangled Linear Polymer Melts: A Molecular-Dynamics Simulation. *J. Chem. Phys.* **1990**, *92* (8), 5057–5086. https://doi.org/10.1063/1.458541.

(29) Souza, P. C. T.; Marrink, S.-J. Martini 3 - Open Beta-Release. 2020.

(30) Marrink, S. J.; Risselada, H. J.; Yefimov, S.; Tieleman, D. P.; De Vries, A. H. The MARTINI Force Field: Coarse Grained Model for Biomolecular Simulations. *J. Phys. Chem. B* **2007**, *111* (27), 7812–7824. https://doi.org/10.1021/jp071097f.

(31) Grunewald, F.; Rossi, G.; de Vries, A. H.; Marrink, S. J.; Monticelli, L. Transferable MARTINI Model of Poly(Ethylene Oxide). *J. Phys. Chem. B* **2018**, *122* (29), 7436–7449. https://doi.org/10.1021/acs.jpcb.8b04760.

(32) Lee, H.; de Vries, A. H.; Marrink, S.-J.; Pastor, R. W. A Coarse-Grained Model for Polyethylene Oxide and Polyethylene Glycol: Conformation and Hydrodynamics. *J. Phys. Chem. B* **2009**, *113* (40), 13186–13194. https://doi.org/10.1021/jp9058966.

(33) LAMMPS - Large-Scale Atomic/Molecular Massively Parallel Simulator, Http://Lammps.Sandia.Gov. *https://lammps.sandia.gov/*.

(34) Plimpton, S. Fast Parallel Algorithms for Short-Range Molecular Dynamics. *J. Comput. Phys.* **1995**, *117* (1), 1–19. https://doi.org/10.1006/jcph.1995.1039.

(35) Plimpton, S.; Pollock, R.; Stevens, M. J. In Particle Mesh Ewald and RRESPA for Parallel Molecular Dynamics Simulations. *Proc. Eighth Siam Conf. Parallel Process. Sci. Comput.* **1997**.

(36) Harmandaris, V. A.; Mavrantzas, V. G.; Theodorou, D. N. Atomistic Molecular Dynamics Simulation of Polydisperse Linear Polyethylene Melts. *Macromolecules* **1998**, *31* (22), 7934–7943. https://doi.org/10.1021/ma980698p.

(37) Humphrey, W.; Dalke, A.; Schulten, K. VMD: Visual Molecular Dynamics. *J. Mol. Graph.* **1996**, *14* (1), 33–38. https://doi.org/10.1016/0263-7855(96)00018-5.

(38) Du, J.; Benmore, C. J.; Corrales, R.; Hart, R. T.; Weber, J. K. R. A Molecular Dynamics Simulation Interpretation of Neutron and X-Ray Diffraction Measurements on Single Phase Y2O3-Al 2O3 Glasses. *J. Phys. Condens. Matter*

2009, *21* (20), 205102. https://doi.org/10.1088/0953-8984/21/20/205102.